Cellulose (2013) 20:3025–3037
DOI 10.1007/s10570-013-0025-1

ORIGINAL PAPER

Different strategies for obtaining high opacity films of MFC with TiO_2 pigments

Raphael Bardet · Mohamed Naceur Belgacem · Julien Bras

Received: 5 July 2013 / Accepted: 12 August 2013 / Published online: 31 August 2013

Abstract The present study examines the production and characterization of opaque solid films made with microfibrillated cellulose (MFC) suspension and titanium dioxide (TiO_2) nanoparticles. Three different strategies were investigated: a blend of (1) MFC and TiO_2 (2) a premix in which TiO_2 particles are used to favor the fibrillation step of MFC and (3) a sol–gel strategy in which TiO_2 particles were directly generated onto the surface of MFC. The different process parameters have been optimized both for the production of MFC and the sol–gel reaction. Gel suspensions containing different ratios of TiO_2 were morphologically and chemically characterized. In order to characterize the size and the nature of the particles, diffraction laser scattering, atomic force microscopy were used while the thermo gravimetric analysis and X-ray diffraction were used to investigate the degradation of MFC for all the three strategies. To highlight the level of dispersion of TiO_2 within the MFC network, scanning electron microscopy in BSE mode has been employed. Finally, the transparence and the mechanical properties of solid films were measured by UV spectrophotometry and tensile tests, respectively. Very good TiO_2 dispersion and high opacity MFC films have been achieved with a very low amount of TiO_2. Thus, the best strategy that takes into account the easiest process for making the hybrids and leading to the high level of opacity with the lowest ratio of TiO_2 is the premix strategy.

Keywords Microfibrillated cellulose · Hybrid nanomaterials · Titanium dioxide · Film opacity

R. Bardet · M. N. Belgacem · J. Bras (✉)
Laboratory of Pulp and Paper Sciences (LGP2), The International School of Paper, Print Media and Biomaterials (Pagora), Grenoble Institute of Technology (INP), UMR CNRS 5518, 461 rue de la Papeterie, BP 65, 38402 Saint Martin d'Hères Cedex, France
e-mail: Julien.Bras@grenoble-inp.fr

Introduction

For the last 20 years, the scientific community has taken a growing interest in the study of cellulose broken down to the nanoscale (Klemm et al. 2011; Dufresne 2012). Among "nanocellulose", two families exist: the nanocrystalline cellulose (NCC) (Marchessault et al. 1961) and the microfibrillated cellulose (MFC) (Turbak et al. 1983) depending of the treatment to which the starting material is subjected, i.e. acidic treatment or mechanical disintegration, respectively. It is generally admitted that NCC and MFC can, respectively, be assimilated to nanoscale "rice-like" and "spaghetti-like" structures. Indeed, NCCs are rod-like crystalline cellulose particles, and can be assimilated to a liquid crystal suspension whereas MFC are flexible, semicrystalline, and have a gel like property in diluted suspensions. Since 2010, several reviews report the different techniques for production, characterization, and end-uses of these promising biobased nanomaterials (Eichhorn et al. 2010; Habibi et al.

2010; Siró and Plackett 2010; Moon et al. 2011; Lavoine et al. 2012). This study will focus on the potential of MFC.

Microfibrillated cellulose has been discovered by Herrick and Turbak groups in 1982 and 1983, respectively (Herrick et al. 1983). The first applications of MFC suspension were as rheology modifier (Turbak et al. 1983), emulsion stabilizer (Andresen et al. 2006; Xhanari et al. 2011), and during the last decade in nanocomposites (Siqueira et al. 2010), biobased films (Fukuzumi et al. 2008; Belbekhouche et al. 2011; Siro et al. 2011; Nakagaito et al. 2010) or aerogels (Jin et al. 2011; Kettunen et al. 2011). More recently, promising results have been found in the field of medical applications, as antimicrobial agents (Martins et al. 2012) or anti-inflammatory biomaterials (Herranen and Lohman 2012). The main properties of MFC are their intrinsic outstanding mechanical properties (4–15 GPa), high specific surface area (40–100 m^2/g) and their high surface density of hydroxyl group. For these reasons and thanks to hydrogen bonds that explain why a gel-like suspensions is achieved at a very low concentration in water, once dried, MFC are entangled with each other to form an entanglement nanoporous network that looks like a solid, usually, transparent film (Spence et al. 2010). In some applications like food, packaging, the opacity is required to ensure light protection of the product and limit food spoilage. In this context, biobased packaging is expected to be a key candidate in such applications, which motivated us to undertake a study aiming at manufacturing of high opacity hybrid film.

Among all the industrially used pigments, titanium dioxide (TiO_2) is one of the most efficient regarding its opacifying and covering effects (Nelson and Deng 2008). However, when TiO_2 particles are not well dispersed and agglomerated in any matrix, their light scattering zones overlap and reduce their opacifying effect. One existing solution consists of using opaque hollow polymeric spheres or core–shell mineral pigments (Alince and Lepoutre 1980; Rennel and Rigdahl 1994; Johnson et al. 1997). In addition, specific binders, extenders or dispersants are also used in order to reduce the agglomeration phenomena, thus providing improvement in the light scattering efficiency (Eckenrode and Fasano 2012). However, with the increasing interest about environmental concerns and due to the rising price of this geolocalized raw material, new solutions are expecting using biobased materials and limiting TiO_2 quantity.

To the best of our knowledge, the process of obtaining a mineral filler/MFC hybrid film has been studied very little and most studies were mainly devoted to barrier and mechanical properties using different biomimetic approaches such as nacres (Wu et al. 2012; Ridgway and Gane 2012; Nypelö et al. 2011; Liu and Berglund 2012). Since the beginning of the current decade, several innovations related to this concept have been patented by the filler suppliers or paper producers. Initially, patents have been mainly developed in order to overcome the drawback of gel-like MFC suspension at a low solid content (Saarikoski et al. 2012; Iotti et al. 2011). This could cause several constrains regarding the process production and application (during mixing, pumping, and coating steps) and commercialization (cost efficiency). None of these studies have focused on the development high opacity MFC films.

Indeed, to the best of our knowledge, there is no reference in the literature dealing in which a combination of TiO_2 filler and MFC to produce opaque films. However, Schütz and coauthors have recently proposed to produce a hybrids composed of MFC and *ex-situ* anatase TiO_2 in order to investigate a potential use for transparent coatings with a good abrasion resistance and photocatalytic UV activity (Schütz et al. 2012). For the production of a MFC/filler hybrid suspension, several strategies can be tested. The first one consists of fibrillating the cellulose fibers directly with abrasive fillers (Husband et al. 2010; Gane et al. 2010), whereas the second deals with adding the inorganic materials after the fibrillation (Laine et al. 2010; Berglund and Liu 2011). Another strategy exists taking into account that cellulosic fibers can act as efficient hydrophilic substrates for the nucleation and growth of inorganic particles in aqueous medium (Barata et al. 2005; Vilela et al. 2010). In a similar way, Marques and coauthors have investigated the way of in situ generation of TiO_2 in the presence of the cellulose fibers (Marques et al. 2006). However, this innovative strategy has never been adapted to MFC.

The present work proposes, for the first time, the determination of the optimal conditions of preparing highly opaque films made of MFC and titanium oxide. Three strategies have been tested and compared as shown in Fig. 1 : (1) a blend of MFC and TiO_2, (2) a premix in

which TiO_2 particles are used as a fibrillation aid of MFC and (3) a sol–gel strategy in which TiO_2 were directly generated onto the MFC surface. The prepared materials have been evaluated in terms of opacity and mechanical resistance and compared with other matrices.

Materials and methods

Materials

Titanium dioxide powders are two commercial grades with two different polymorphisms, a rutile TiO_2 (Tiona©, Millennium Chemicals, England) and an anatase TiO_2 (Ti-Pure®RPS Vantage®, Dupont, USA). Their average diameter D_{50} measured by laser granulometery (1190 Particle Size Analyzer®, Cilas, France) are $D_{50} = 0.37 \pm 0.07$ μm and 0.40 ± 0.05 μm for rutile and anatase, respectively. hydrated titanium (IV) oxysulphate (Sigma-Aldrich, France) was used as precursor for the sol–gel reaction. Commercial organic binders used were potato starch (Perfectafilm®, Avebe, Holland), sodium carboxymethylcellulose (Blanose® Cellulose Gum, Ashland, USA) and Polyvinyl alcohol (Mowiol® 28-99, Kuraray, Japan). Potato starch, CMC and PVOH were cooked and stored according to the supplier recommendations. Deionized water was used in all experiments.

MFC production

MFC was prepared from a dried commercial sulphite softwood-dissolving pulp (Domsjö Cellulose Plus®, Domsjö, Sweden) using disintegration, enzymatic pretreatment and fine grinding treatment. First, the pulp suspension (10 % w:w) was beaten in a PFI mill until 60,000 revolutions according to ISO 5264-2:2002 standard. Then, the refined bleached fibers were diluted to a 5 % w:w consistency suspension and mixed with a selected enzymatic cocktail of cellulase (0.6 % w:w based on dried pulp). The resulting suspensions were incubated during 2 h at 50 °C and buffered with sodium acetate/acetic acid at a pH = 5. The enzyme used was a monocomponent endoglucanase (Celluclast 1.5L®, Sigma-Aldrich, France) with an enzymatic activity of 700 ECU/g. The enzymatic reaction was inhibited by heating the suspension at 90 °C for 15 min. Finally, the mixtures were diluted with deionized water to a 2.5 % consistency, and then passed through an ultra-fine grinder (Supermasscolloider MKCA6-2®, MASUKO SANGYO CO, LTD, Japan). The suspensions were passed 60 times between a static and a rotating silicon carbides grindstones (MKG-C/46#, MASUKO SANGYO CO, LTD, Japan) with a gap corresponding to the 0-motion point and at a rotating speed of 1,500 rpm. At the end of the production, a small quantity of Chloroform (0.01 w:w %) was added to the suspension to prevent microbial growth during storage at 4 °C.

Preparation of MFC and TiO_2 hybrid suspensions

The blend of hybrid MFC (strategy 1) was prepared by mixing with a homogenizer (UltraTurrax T8®, IKA, France) abrasive TiO_2 particles with the MFC suspension at 10,000 rpm for 5 min. The dry content of the suspension thus obtained was adjusted to 2.5 % (w:w).

The protocol of the premix (strategy 2) was adapted from the initial protocol for MFC. Thus, TiO_2 powder was added before the suspension fibrillation with the ultra-fine grinder. The consistency of the obtained suspension was adjusted to 2.5 % and ground under the same operation parameters.

The sol–gel reaction (strategy 3) was performed in MFC suspension in order to generate 20 % (w:w) of TiO_2 particles onto the MFC surface. The sol–gel reaction was carried out in a 5 L glass flask, where 67.1 g of precursor (Titanium Oxysulphate) was dissolved with 3,000 g of the never-dried MFC suspension. The amount of the precursor was set at 0.74 g per gram of dried MFC. The mixture was heated at 50 °C under constant mechanical stirring at 500 rpm for 100 min. Then, the hybrid suspension was washed following at least three successive centrifugations at 400 Rotation Centrifugal Force and 10 °C for 10 min, in order to remove the residual sulfuric acid and the precursor. The dry content of the suspension thus obtained were adjusted to 2.5 %.

MFC/TiO_2 film preparation

10 g of hybrid suspensions at 2.5 % w:w consistency were diluted in 40 ml of water and homogenized with UltraTurrax during 3 mn at 10,000 rpm. Then MFC films were casted in Teflon molds (6 cm diameter) and left to dry during 3 days at room conditions (50 % RH, 23 °C). For each series, five solid films of 30 g/m^2 were thus obtained.

Nanoparticle characterization

Individual nanoparticles were imaged using Atomic Force Microscope, AFM, (Nanoscope III®, Veeco, Canada). All samples were previously diluted at 10^{-4} % and a drop of 0.2 ml was deposited onto freshly cleaved Mica substrates and dried overnight under room conditions. Each sample was characterized in tapping mode with a silicon cantilever (OTESPA®, Bruker, USA) at four different locations and two different scanning areas: 10×10 and 3×3 μm^2. Both topographical and phase images were captured and images were subjected to first order polynomial flattening to reduce the effects of bowing and tilt.

Dynamic Light Scattering (DLS) was used to measure the size of in situ nanoparticles (Vasco® I, Corduan Technologies, France). All the samples were previously diluted in DI water at 10–2 % (w:w). The analysis mode is the cumulative method and two parameters were taken into account, namely: the average size (z*) and the polydispersity index (PDI). For each sample, 10 acquisitions were performed and each measurement was replicated 3 times.

Hybrid films characterization

Before characterization, the films were conditioned in a constant temperature and humidity chamber kept at 25 °C with 50 % of relative humidity, for at least 48 h. E-SEM (Environmental Scanning Electron Microscope) in backscattered electron mode (BSE) was used (Quanta 200©, FEI, Japan). Pictures were then treated using image treatment software (ImageJ©, NIMH, USA). The films were previously conditioned and coated with gold/palladium and observed using an applied tension of 15 kV. The cross-section pictures were obtained by a cryofracture of dried hybrid films with liquid nitrogen.

The thicknesses of the films were determined from the cross-section pictures of E-SEM micrographs. For each film, 12 measurements were performed at four different locations whereas the basis weight was evaluated using ISO-536:1995 standard. The film density was calculated by dividing the basis weight by the film thickness.

Film transparency was estimated with a UV spectrophotometer (UV 1800®, Shimadzu, Japan). The absorption of the solid film has been measured at a wavelength of 550 nm that corresponds to the maximum wavelength absorption peak of TiO_2. For each sample, 3 different measurements and 10 scans have been recorded.

The mechanical properties of the films were measured using universal testing machine (Model 4465®, Instron Engineering Corporation, US). The evaluation of the Young's modulus, tensile strength and the elongation were established following the ISO-1924-2:2008 standard. For each film, six specimens with a 15 mm in width and 50 mm in length have been submitted to a 20 mm/min constant speed of elongation. All mechanical tests have been repeated 6 times for each sample.

Field-emission scanning electron microscope (FE-SEM) was used to observe the nanostructure of the surface of hybrid films (Ultra 55©, Zeiss, Germany). The films were covered with carbon tape and coated with a 2 nm layer of gold/palladium to ensure the conductivity of all samples. The accelerating voltage (EHT) was 3 kV for a working distance of 6.4 mm.

The thermal degradation of cellulosic samples was monitored by TGA (thermo-gravimetric analyzer-STA 6000®, Perkin Elmer Instruments, England). The weight loss and heat flow curves were recorded for a 30 mg sub-sample at a heating rate of 10 °C/min in the temperature range of 30–950 °C under oxidizing atmosphere (air). For TG analysis, the experiment have been duplicated and averaged.

The X-ray diffraction (XRD) patterns were measured for hybrid films with X-ray diffractometer (PANanalytical®, X'Pert PRO MPD). The operating conditions for the refractometer were Cu, Kα radiation (1.5418 Å), 2θ Bragg angle between 5 and 60°, step size of 0.067°, and a counting time of 90 s. The cellulose crystallinity index (CI) was evaluated using empirical method developed by Segal et al. (1959). For each XRD patterns, the experiments have been duplicated and then averaged.

Results and discussions

Nanoparticle characterization: MFC and TiO_2

After refining, enzymatic pretreatment and fine grinding process, MFC gel suspensions were achieved. The characterization of this material is a key challenge because it makes easy the comparison with other elements reported in several scientific papers and

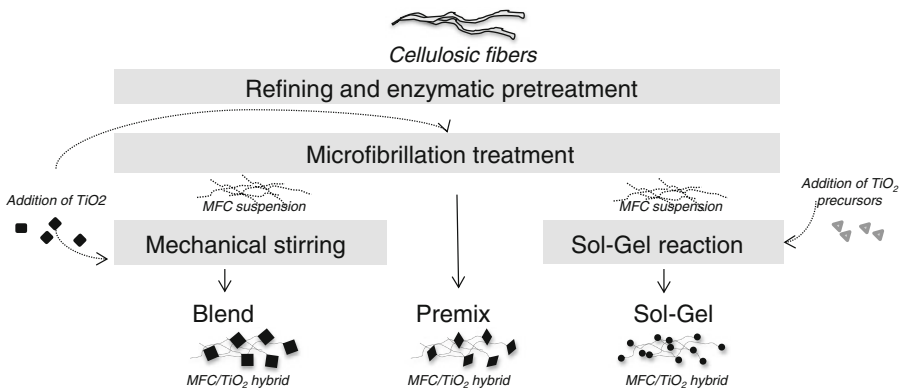

Fig. 1 Schematic representation of the 3 strategies used for MFC/TiO_2 hybrid films

could rationalize the obtained results (both mechanical and optical). Indeed the term MFC still includes a large range of materials with different dimensions and heterogeneity (Klemm et al. 2009). In our case, the diameter dimension has been calculated from the average MFC thickness of AFM pictures (Fig. 2b) and a value of 45 ± 15 nm was obtained, which is in agreement with recently available literature (Lavoine et al. 2012). The uniformity and homogeneity of MFC has been visually checked thanks to gel like structure of the suspension (Fig. 2a) indicating the absence of microscopic cellulosic fibers.

Dispersion of TiO_2 into MFC hybrid films

The main target of this study is to obtain opaque films with the lowest amount of opacifying mineral particles. As shown in Fig. 3, it has been found that, when TiO_2 particles are simply mixed with a MFC suspension (strategy 1), the solid film thus obtained presents a very low transparency in comparison to the same film obtained without TiO_2 that can be assimilated as a homogenous and transparent film. It is assumed that the difference in opacity of two films is mainly due to the well-known difference of refractive index (RI) between TiO_2 (RI = 2.55–2.73) and cellulose (RI = 1.53). The opacifying effect is proportional to the difference between the refractive index of the pigment and the medium in which it is dispersed. That is one of the reasons that explain the TiO_2 –containing film opacity.

In order to establish the best range of TiO_2 for producing MFC hybrid films, the influence of the polymorphism type and the amount of TiO_2 on the film transparency has been performed, as presented in Fig. 3. As expected, the transparency of film strongly decreases with the amount TiO_2. However, the absorbance reaches a plateau value at a volume fraction of 20 % of TiO_2 (41 % w:w). Beyond 20 %, TiO_2 particles are agglomerated and crowded which limits their light scattering properties. In our experiments, a slight difference have been find between rutile and anatase starting from a 5 % (v:v) content. This may come from a difference in mean diameter and refractive indices, i.e., 2.55 and 2.73, for anatase and rutile, respectively. Nevertheless, it assumed the difference could be considered negligible in this study due to the method used for the evaluation of the transparency. This is why, anatase particles have been chosen for the rest of this study because the sol–gel reaction generates only this polymorphic form (Kolen'ko et al. 2003). Moreover, such a solution is cost-effective.

The grey level contrast in E-SEM BSE (Back Scattering Electron) mode of cross-section of hybrid film (Fig. 4) shows the chemical difference between the MFC network (organic) and TiO_2 particles (mineral). This highlights the excellent dispersion of mineral particles in the whole thickness of the film. It can be observed that TiO_2 particles are well distributed without sedimentation or agglomeration within the thickness of solid film. The absence of sedimentation and the excellent distribution of TiO_2 particles can be explained by the MFC gel-like structure when the suspensions are produced and their ability to form a nanoporous network that is able to well-disperse small particles such as those of TiO_2. Thus, these micrographs establish that mineral particles can be easily dispersed in a MFC medium to form an opaque solid film.

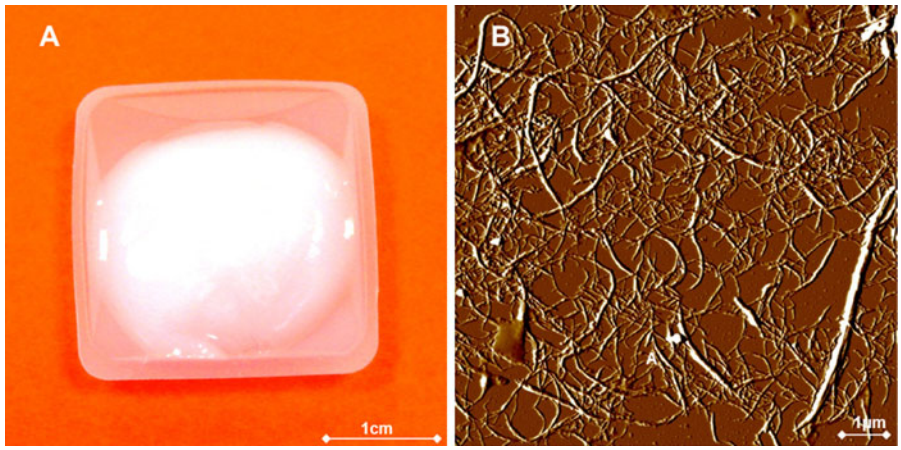

Fig. 2 Characterization of the MFC. **a** To the gel-like suspension of MFC at 2.5 % of consistency. **b** Same suspension observed through AFM at a scanning area of 10 × 10 µm^2 in TAPPING mode (amplitude error)

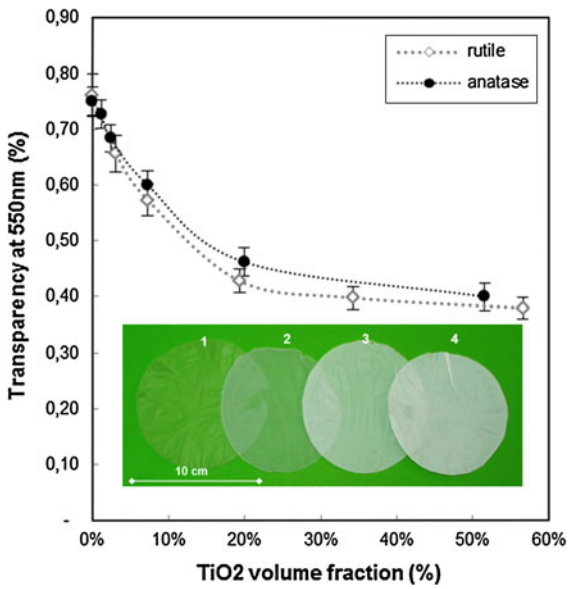

Fig. 3 Transparency of a 30 g/m^2 MFC solid film as a function of the volume ratio of TiO_2. Comparison between rutile (*diamond*) and anatase (*circle*) polymorphs. *Pictures 1–4* corresponds to MFC films with an increasing amount of rutile TiO_2 (0, 2, 7 and 20 %)

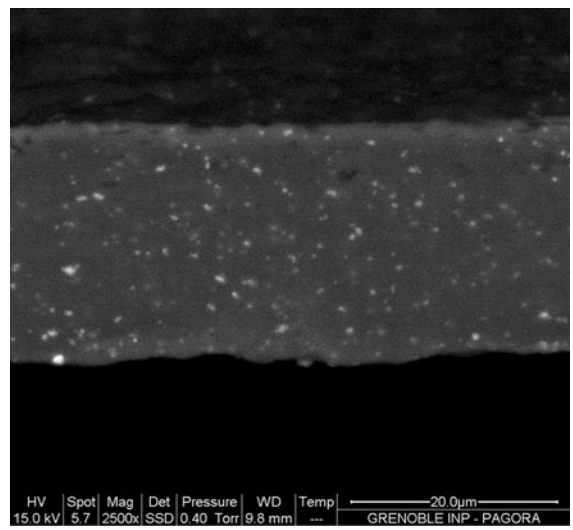

Fig. 4 E-SEM (BSE mode) of cross-sectional pictures of a MFC hybrid film (10 % of TiO_2)

Comparison of MFC with other polymers

To confirm the benefit of using MFC as a potential matrix for opaque film, the mechanical and optical properties have been compared to other classical matrix used in opacity applications such as PVOH, CMC and starch. The main results are reported in Table 1.

The mechanical resistance is generally higher for MFC whatever the ratio of TiO_2. By comparing the specific Young's modulus (by dividing E by the film density), MFC films are systematically stronger than those prepared from CMC (+6 to 20 %) and PVOH (+19 to 36 %) whereas films made of starch are 3–4 times weaker than those made of MFC. The results obtained for pure films are really close to the values given in the literature, i.e., Young Modulus for MFC of about 15–20 MPa (Syverud and Stenius 2009; Siro et al. 2011; Plackett et al. 2010). Some differences between the values found in the literature could

Table 1 Main features of opaque films made with different matrices with 0, 20 and 50 % TiO_2

Matrix	Ratio of TiO_2 (w:w %)	Density		Strain at break (%)		Force at break (kN/m)		Specific young modulus (GPa)		Transparency (%)	
PVOH	0	1.3	(0.1)	7.30	(0.20)	2.90	(0.03)	9.0	(0.7)	93.9	(1.3)
CMC		1.6	(0.3)	2.30	(0.07)	2.60	(0.05)	9.2	(1.3)	91.0	(1.2)
Starch		1.2	(0.0)	2.50	(0.03)	1.20	(0.05)	2.7	(0.4)	96.4	(0.8)
MFC		1.0	(0.2)	4.50	(0.03)	3.60	(0.06)	12.3	(1.0)	76.1	(1.2)
PVOH	20	1.4	(0.1)	5.20	(0.19)	0.60	(0.10)	2.6	(0.5)	56.4	(0.5)
CMC		1.7	(0.2)	1.65	(0.06)	0.80	(0.10)	2.6	(0.1)	72.9	(0.5)
Starch		1.3	(0.2)	1.30	(0.15)	0.20	(0.00)	1.3	(0.0)	53.9	(1.5)
MFC		1.2	(0.2)	3.00	(0.10)	0.60	(0.05)	5.2	(0.0)	38.7	(0.3)
PVOH	50	1.8	(0.1)	2.87	(0.10)	0.10	(0.01)	1.5	(0.8)	38.4	(0.7)
CMC		2.0	(0.3)	2.30	(0.22)	0.10	(0.03)	3.4	(0.3)	57.7	(2.3)
Starch		1.7	(0.3)								
MFC		1.6	(0.1)	2.30	(0.22)	0.20	(0.03)	3.6	(0.3)	30.8	(1.5)

Values into brackets refer to standard deviation

originate from the protocols used for producing MFC and for MFC solid films making and characterization.

As expected, for high ratio of mineral particles (50 % of TiO_2), a significant reduction for all mechanical properties is observed, because the introduction of TiO_2 particles create too many weak points in the film and limits hydrogen bonds. Such a phenomenon is more pronounced in the case of the force at break, which is divided by 10 when 50 % TiO_2 is added. Such a dramatic decrease is due to the fact that MFC films are nano-porous films contrary to other common polymer matrices.

Concerning the films transparency, which is the key parameters of this study, i.e., it was found that films made of MFC are systematically more opaque than the other ones. Only films filled with 20 % of TiO_2, were highly opaque and a sharp drop (from 76 to 39 %) of the transparency was measured, whereas for PVOH-, CMC- and starch-based-films made with the same percentage of TiO_2, the transparency is still high. Moreover, even when increasing the amount of TiO_2 (up to 50 %), the obtained films did not reach a similar low transparency. In other words, for producing opaque films with the same optical properties, 60 % of TiO_2 can be saved if PVOH or CMC is replaced by MFC. Such a feature is of high importance from industrial point of view, since such films would contain a lower quantity of TiO_2 and display at least the same the mechanical properties. Alternatively, a weight reduction of the film can be also envisaged. This confirms the impact of the nanofilament networks which enhances the good dispersion of TiO_2, as recently patented (Bras et al. 2012).

Comparison of the different strategies for mixing TiO_2 with nanocellulose

Another target of this study was to check the influence of different strategies of producing MFC-TiO_2 films. As shown previously, MFC hybrid films promote the opacifying effect of TiO_2 and offering very good mechanical. However, with a process consideration and for further commercial application such as for packaging films or coating, the mixing process of TiO_2 must be optimized. Figure 1 presents the three different approaches studied: (1) the blend of MFC and TiO_2, (2) the premix in which TiO_2 particles are used to favor the fibrillation step of MFC, and (3) the sol–gel strategy in which TiO_2 were in situ generated onto the surface of MFC. As described in the experimental section, the blend and the premix strategies are similar regarding the production process. However, the main benefit of premixing the suspension with abrasive fine particles is decreasing the number of treatment cycles thus leading to significant energy consumption saving. Indeed, the high abrasiveness of TiO_2 promotes the cellulosic fiber (micro)-fibrillation treatment. This is in agreement with a recent patent using similar strategy for limiting energy consumption but using calcium carbonate as abrasive particles (Gane et al.

2011). In our case, only 15 recirculation cycles were needed compared to 60 recirculations needed for the production of neat MFC. This also highlights a new benefit of using a fine grinder instead of other conventional technologies, such as homogenizer or microfluidizer (Spence et al. 2011) for the production of MFC. Indeed, the addition of such abrasives particles is only possible by using mechanical disintegration and not adapted to machines based on high-shearing principle.

Concerning the sol–gel reaction (strategy 3), following Marques and coworkers study, in which a TiO_2/cellulose fibers hybrid have been prepared in acidic medium (Marques et al. 2006). Thus, the hydrothermal conditions have been adapted for MFC for two mains reasons: the final ratio of TiO_2 is too high considering the optimal ratio previously established and reported in the experimental section. In addition, the accessibility of nanocellulose should clearly differ from macroscopic cellulose fibers mainly due to its high surface area. Figure 5 highlights the nucleation and growth steps of TiO_2, as a function of the reaction time and in the absence of cellulosic substrates. As expected, the average diameter of TiO_2 particles significantly increases with increasing the reaction time for the first 40–50 min of reaction. Then, the particles size reaches a plateau value at around 300 nm. A similar trend was also found considering the peak intensity at 550 nm, which corresponds to maximum absorption wavelength of TiO_2. AFM images at 3 different reaction times (3, 60 and 120 min) also confirm the in situ production TiO_2. This also gives an idea of the morphology of generated TiO_2 particles that are rather clustered particles. In order to prevent the hydrolysis of cellulose during the sol–gel reaction, the shortest reaction time has been chosen while ensuring an optimum particles size for the light scattering (about 300 nm). For these reasons, a reaction time of 100 min (instead of 270 min) and a reaction temperature of 50 °C (instead of 70 °C) have been selected. To reduce the hydrolysis of cellulose, sulphuric acid have been also removed from the initial protocol. Proofs of the sol–gel reaction have been achieved by TGA, XRD and UV–visible characterization which will be detailed later. An AFM picture of TiO_2 particles generated onto MFC is presented in Fig. 6. Actually, the sol–gel strategy is still the most complicated to carry out because it requires several production steps: the production of nanocellulose, the sol–gel reaction in acid medium and finally a neutralization step. However, one of the main benefits of this strategy is the possibility to tune the size of generated TiO_2 particles.

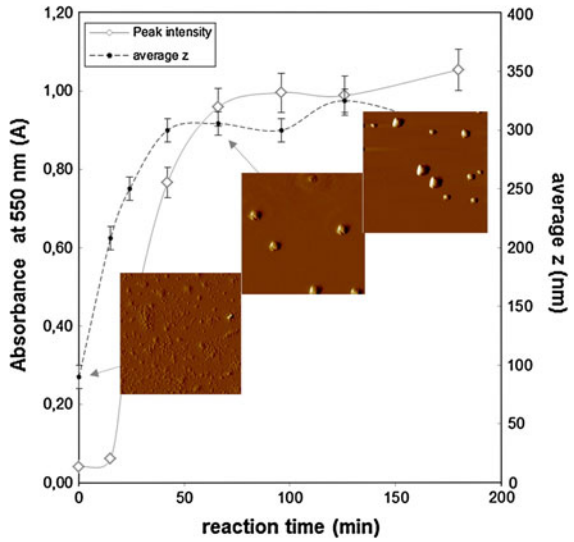

Fig. 5 Peak intensity (*diamond*) and average z (*circle*) as a function of the sol–gel reaction time. *Pictures* correspond to the AFM scan imaging in tapping mode (amplitude error, 3×3 μm^2,) at three reaction times (3, 66 and 126 min, respectively)

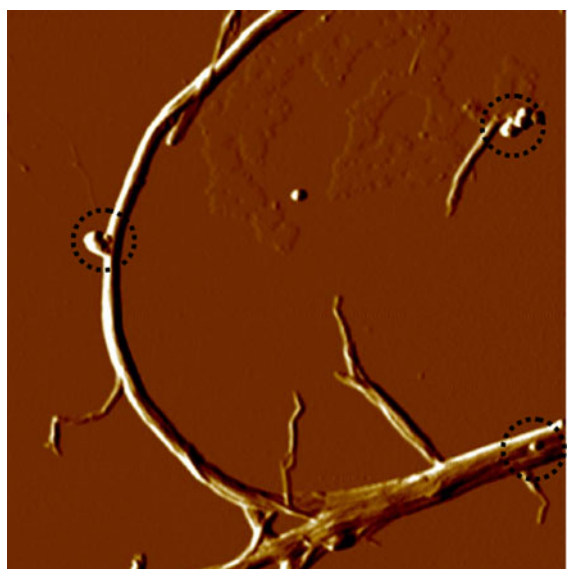

Fig. 6 AFM image of individualized MFC in which in situ TiO_2 (*dotted circle*) have been generated through the sol–gel reaction at a scanning area of 3×3 μm^2 in TAPPING mode (amplitude error)

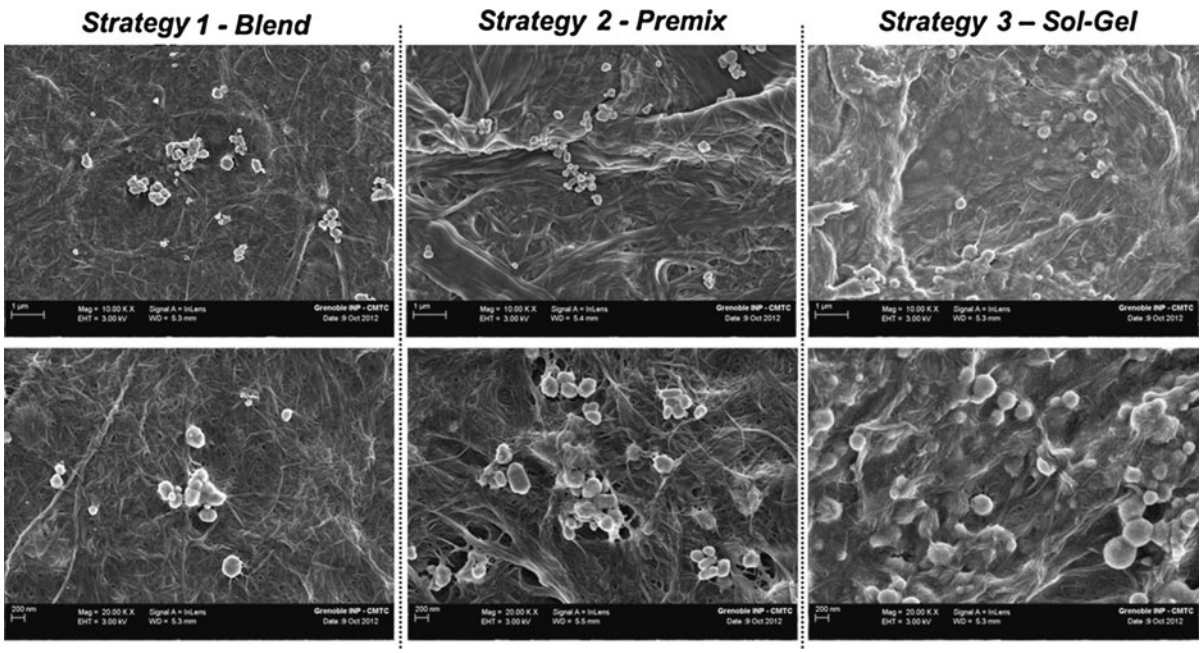

Fig. 7 FE-SEM pictures of hybrid films at two magnification level (*Up*: ×10,000 and *Down*: ×20,000). Comparison between the surface of blend, premix and hybrid films

Comparison of the final properties of MFC-TiO_2 films made with different strategies

After having briefly discussed about the production process of MFC hybrid suspension, the end-use properties of the different hybrid films have been compared in terms of mechanical resistance and optical properties. As shown in FE-SEM micrographs of hybrid films (Fig. 7), *ex-situ* TiO_2 particles (strategy 1 and 2) are trapped into the nanoporous network of entangled MFC. *In-situ* TiO_2 particles (strategy 3) are well dispersed with spherical shape and in this case they are considered to be physically adsorbed at the surface of MFC (Fig. 7). This confirms that MFC can act as nucleation sites for TiO_2 particles during the sol–gel reaction. The average diameter of individual TiO_2 observed by FE-SEM particles is about 290 ± 10, 225 ± 15 and 325 ± 130 nm for blend, premix and sol–gel hybrid films, respectively. High shearing and abrasiveness of ceramic plate of the fine grinding may have led to a reduction of TiO_2 particle size during the fibrillation step (strategy2). Concerning MFC, the average width of MFC used for blend strategy is 46 ± 11 nm as already shown by AFM imaging. Once the sol–gel reaction is performed, the width (30 ± 5 nm) decreases due to acidic conditions. However, these values are still in the nano-range, contrary to those detected in the premix MFC. Indeed, due to a lower number of recirculation cycles (15 instead of 60), the presence of some microscopic fibers bigger than 100 nm were detected. Both mean diameter and standard deviation with a width of 180 ± 90 nm were increased. The difference between MFC sizes would be taken into account for mechanical and optical properties analysis. Mechanical and optical properties are reported in Table 2.

The blend and premix hybrid films have similar properties whereas significant decreases are found for hybrid films both in terms of mechanical properties (−60 %) and transparency (−40 %). Such results point out that there is a slight chemical degradation of cellulose during the sol–gel reaction giving rise to the weakening of the films properties. In addition, the lowest opacity obtained through sol–gel strategy can be explained by two main reasons. As mentioned above, to prevent the degradation of cellulose, the reaction time of the sol–gel reaction have been shortened. So the reaction seems to be uncompleted (some TiO_2 precursors remains) and the generated anatase TiO_2 are not fully crystallized. In addition, a

Table 2 Main features of hybrid MFC films

Strategy	Weight ratio of TiO_2 (%)		Density		Strain at break (%)		Force at break (kN/m)		Specific young modulus (GPa)		Transparency	
Blend	17.4	(0.3)	1.2	(0.2)	3	(0.3)	0.60	(0.05)	5.2	(0.1)	38.7	(0.1)
Premix	17.2	(0.5)	1.1	(0.1)	3.0	(0.2)	0.80	(0.02)	5.5	(1.3)	40.3	(0.5)
Hybrid	17.5	(0.8)	1.5	(0.1)	0.5	(0.2)	0.10	(0.02)	1.5	(0.4)	55.0	(0.4)

Values into brackets refer to standard deviation

higher density of the sol–gel films (+20 %) have been measured which is directly related to a reduction of the internal porosity which affects the opacity of the film.

As shown in Fig. 8, TG (thermo-gravimetric) curves highlight the degradation of the cellulose due to the sol–gel reaction. This pyrolysis degradation starts at 238 °C for hybrid films whereas it starts over 300 °C for blend and premix counterparts. The trend of the curve obtained for blend and premix hybrid film is similar to that obtained with neat MFC (not presented) which indicates there is no chemical modification of cellulose. The analysis of derived TGs (not presented) gives a slower rate of the pyrolysis process for the hybrid strategy. These results confirm that the sol–gel reaction in acid medium tend to cause a partial hydrolysis of MFC, which explains the weakening of sol–gel film in comparison to blend and premix homologues. Over 600 °C, the residual mass is between 17 and 18 %. This value can be associated as the inorganic part present in the hybrid films, i.e., the ratio of anatase TiO_2.

The XRD patterns of hybrid films presented in Fig. 9 are strictly the same for premix and blend strategy indicating that there is no modification or rearrangement of cellulose structure in the presence of *ex-situ* TiO_2, whatever the strategies. Fine peaks are observed at 25.3° (1,0,1), 37.0° (0,0,4), 47.5° (2,0,0), 53.3° (105) and 54.4° (2,1,1) which confirms the presence of highly crystallized anatase TiO_2. The pattern of sol–gel hybrid film is different with anatase broader and smaller peaks of TiO_2. In addition, new peaks can be identified at 11.5°, 15.8°, 20.7° and 29.3°, this peaks are the signature of hydrated Titanium(IV) Oxysulphate used as the precursor, thus confirming that residual amount of the precursors is present in the final film. Residues of precursor and low crystallization

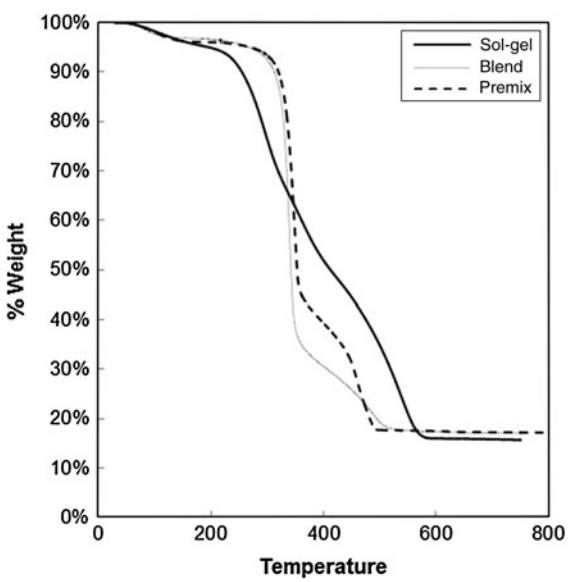

Fig. 8 TG curves for hybrid films (TiO_2 20 % w:w) for a 30 mg sub-sample at a heating rate of 10 C/min in oxidizing atmosphere in the temperature range of 30–950 °C. Comparison between blend, premix and sol–gel strategies

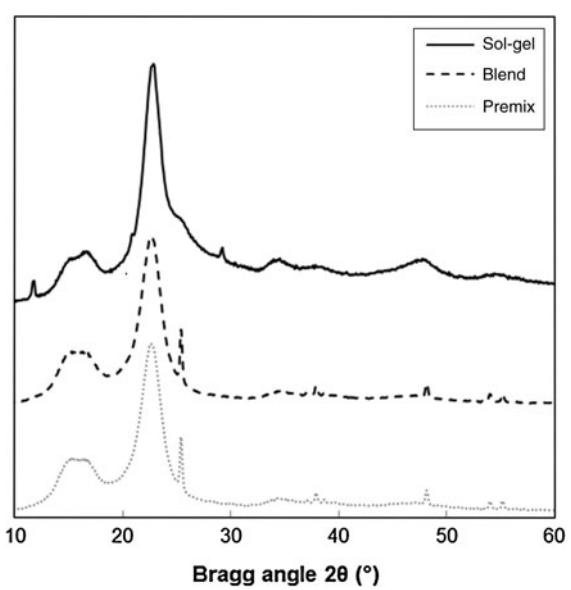

Fig. 9 XRD patterns of anatase TiO_2/MFC films. Comparison between blend, premix and hybrid strategies

of TiO_2 during the reaction explain the highest transparency of the solid film made by in situ TiO_2 route, in comparison to the *ex situ* TiO_2 strategy, in which the titanium oxide particles are well-crystallized during the calcination treatment. According to XRD pattern, The CI (crystallinity index) of cellulose is 82.0 and 81.6 % for premix and blend hybrid films, respectively. For sol–gel films, the CI of cellulose is close to 86.0 %. The higher crystallinity index confirms the hydrolysis of the amorphous part of the cellulose during the sol–gel, as already detected by TG analysis.

Among the three strategies studied to produce an opaque MFC film, premixing solid and abrasive particles with the cellulose fibers (strategy 2) is the most promising by considering the end-use properties and the process for manufacturing these hybrid films.

Conclusions and perspectives

One target of this study was to obtain opaque solid film using TiO_2 particles dispersed in MFC network. This was very successful because a very small amount of TiO_2 (starting from 5 %) is needed to achieve high opacity film. Based on the gel-like properties of MFC suspensions and the ability of MFC to form a well entangled nanoporous network, spherical shape nanoparticles could be trapped and physically dispersed within the thickness of the MFC films. Moreover, such nanocellulose network is even better than continuous films with TiO_2 and classic matrices, concerning the opacity and the mechanical properties of the ensuing materials. Three innovative strategies for mixing TiO_2 and MFC have been proposed and compared for the first time. The blend (strategy 1) and the premix (strategy 2) give the best results regarding both mechanical and optical properties. The premix can be considered as the best solution regarding the process manufacturing.

Even if, the sol–gel reaction (strategy 3) permits to tune the size of TiO_2 particles and favor their physical adsorption, this also leads to a partial hydrolysis of cellulose. The thus obtained hybrid films are not suitable to prepare opaque materials. However, other perspectives can be investigated due to the excellent homogeneity and dispersion of semi-crystalline anatase TiO_2. This study proposes different solutions for obtaining highly opaque hybrid MFC films and opens up the prospect to a new generation of opaque films for light barrier packaging or printed electronics.

Acknowledgments The authors gratefully acknowledge *Papeteries du Léman*, and the French National Research Agency (ANRT) for the financial and material support for the PhD thesis. We would like to thank Berthine Khelifi (Grenoble Institute of Technology) for her expertise in providing E-SEM and FE-SEM imaging and Stéphane Coindeau (Grenoble Institute of Technology) for undertaking XRD analysis.

References

Alince B, Lepoutre P (1980) Light-scattering of coatings formed from polystyrene pigment particles. J Colloid Interface Sci 76(1):182–187. doi:10.1016/0021-9797(80)90284-2

Andresen M, Johansson L-S, Tanem BS, Stenius P (2006) Properties and characterization of hydrophobized microfibrillated cellulose. Cellulose 13(6):665–677. doi:10.1007/s10570-006-9072-1

Barata MAB, Neves MC, Pascoal Neto C, Trindade T (2005) Growth of BiVO4 particles in cellulosic fibres by in situ reaction. Dyes Pigm 65(2):125–127. doi:10.1016/j.dyepig.2004.07.005

Belbekhouche S, Bras J, Siqueira G, Chappey C, Lebrun L, Khelifi B, Marais S, Dufresne A (2011) Water sorption behavior and gas barrier properties of cellulose whiskers and microfibrils films. Carbohydr Polym 83(4):1740–1748. doi:10.1016/j.carbpol.2010.10.036

Berglund L, Liu A (2011) Strong nanopaper with high oxygen barrier properties, comprising nanocomposites of microfibrillated cellulose nanofibers and layered clay and manufacture and use thereof. WO2011059398A1

Bras J, Belgacem MN, Bardet R, Dumas J, Agut P (2012) Couche d'opacification d'un support papier. FR1258093

Dufresne A (2012) Nanocellulose, from nature to high performance tailored materials. doi:10.1515/9783110254600

Eckenrode HM, Fasano DM (2012) Shining new light on opaque polymer. JCT Coatings Tech 9(8):40

Eichhorn SJ, Dufresne A, Aranguren M, Marcovich NE, Capadona JR, Rowan SJ, Weder C, Thielemans W, Roman M, Renneckar S, Gindl W, Veigel S, Keckes J, Yano H, Abe K, Nogi M, Nakagaito AN, Mangalam A, Simonsen J, Benight AS, Bismarck A, Berglund LA, Peijs T (2010) Review: current international research into cellulose nanofibres and nanocomposites. J Mater Sci 45(1):1–33. doi:10.1007/s10853-009-3874-0

Fukuzumi H, Saito T, Iwata T, Kumamoto Y, Isogai A (2008) Transparent and high gas barrier films of cellulose nanofibers prepared by TEMPO-mediated oxidation. Biomacromolecules 10(1):162–165. doi:10.1021/bm801065u

Gane PAC, Schoelkopf J, Gantenbein D, Schenker M, Pohl M, Kuebler B (2010) Process for the production of nanofibrillar cellulose suspensions. WO2010112519A1

Gane PAC, Schenker M, Subramanian R, Schoelkopf J (2011) Process for production of nano-fibrillar cellulose gel composites for wide variety of applications. EP2386683A1

Habibi Y, Lucia LA, Rojas OJ (2010) Cellulose nanocrystals: chemistry, self-assembly, and applications. Chem Rev 110(6):3479–3500. doi:10.1021/cr900339w

Herranen K, Lohman M (2012) Anti-inflammatory effect of microfibrillated cellulose for treatment of skin disorders. WO2012107648A1

Herrick FW, Casebier RL, Hamilton JK, Sandberg KR (1983) Microfibrillated cellulose: morphology and accessibility. J Appl Polym Sci: Appl Polym Symp 37:797–813

Husband JC, Svending P, Skuse DR, Motsi T, Likitalo M, Coles A (2010) Paper filler composition. WO2010131016A2

Iotti M, Gregersen OW, Moe S, Lenes M (2011) Rheological studies of microfibrillar cellulose water dispersions. J Polym Environ 19(1):137–145. doi:10.1007/s10924-010-0248-2

Jin H, Kettunen M, Laiho A, Pynnönen H, Paltakari J, Marmur A, Ikkala O, Ras RHA (2011) Superhydrophobic and superoleophobic nanocellulose aerogel membranes as bioinspired cargo carriers on water and oil. Langmuir 27(5):1930–1934. doi:10.1021/la103877r

Johnson RW, Thiele ES, French RH (1997) Lightscattering efficiency white pigments: an analysis of model core-shell pigments vs. optimized rutile TiO2. Tappi J 80(11):233–239

Kettunen M, Silvennoinen RJ, Houbenov N, Nykanen A, Ruokolainen J, Sainio J, Pore V, Kemell M, Ankerfors M, Lindstrom T, Ritala M, Ras RHA, Ikkala O (2011) Photoswitchable superabsorbency based on nanocellulose aerogels. Adv Funct Mater 21(3):510–517. doi:10.1002/adfm.201001431

Klemm D, Schumann D, Kramer F, Heßler N, Koth D, Sultanova B (2009) Nanocellulose materials—different cellulose. Different functionality. Macromol Symp 280(1):60–71. doi:10.1002/masy.200950608

Klemm D, Kramer F, Moritz S, Lindstrom T, Ankerfors M, Gray D, Dorris A (2011) Nanocelluloses: a new family of nature-based materials. Angewandte Chemie-International Edition 50(24):5438–5466. doi:10.1002/anie.201001273

Kolen'ko YV, Burukhin AA, Churagulov BR, Oleynikov NN (2003) Synthesis of nanocrystalline TiO2 powders from aqueous TiOSO4 solutions under hydrothermal conditions. Mater Lett 57(5–6):1124–1129. doi:10.1016/s0167-57(02)00943-6

Laine J, Oesterberg M, Delphine M, Pohjola L, Sinisalo I, Kosonen H (2010) Method for producing furnish and paper by treatment with cationic polyelectrolyte and nanofibrillated cellulose. WO2010125247A2

Lavoine N, Desloges I, Dufresne A, Bras J (2012) Microfibrillated cellulose—its barrier properties and applications in cellulosic materials: a review. Carbohydr Polym 90(2):735–764. doi:10.1016/j.carbpol.2012.05.026

Liu A, Berglund LA (2012) Clay nanopaper composites of nacre-like structure based on montmorrilonite and cellulose nanofibers—improvements due to chitosan addition. Carbohydr Polym 87(1):53–60. doi:10.1016/j.carbpol.2011.07.019

Marchessault RH, Morehead FF, Koch MJ (1961) Some hydrodynamic properties of neutral suspensions of cellulose crystallites as related to size and shape. J Colloid Sci 16(4):327–344

Marques PAAP, Trindade T, Neto CP (2006) Titanium dioxide/cellulose nanocomposites prepared by a controlled hydrolysis method, vol 66, vols 7–8. Elsevier, Kidlington; ROYAUME-UNI

Martins NCT, Freire CSR, Pinto RJB, Fernandes SCM, Neto CP, Silvestre AJD, Causio J, Baldi G, Sadocco P, Trindade T (2012) Electrostatic assembly of Ag nanoparticles onto nanofibrillated cellulose for antibacterial paper products. Cellulose 19(4):1425–1436. doi:10.1007/s10570-012-9713-5

Moon RJ, Martini A, Nairn J, Simonsen J, Youngblood J (2011) Cellulose nanomaterials review: structure, properties and nanocomposites. Chem Soc Rev 40(7):3941–3994. doi:10.1039/c0cs00108b

Nakagaito AN, Nogi M, Yano H (2010) Displays from transparent film of natural nanofibers. MRS Bull 35(3):214–218. doi:10.1557/mrs2010.654

Nelson K, Deng Y (2008) Enhanced light scattering from hollow polycrystalline TiO2 particles in a cellulose matrix. Langmuir 24(3):975–982. doi:10.1021/la702582u

Nypelö T, Österberg M, Laine J (2011) Tailoring surface properties of paper using nanosized precipitated calcium carbonate particles. ACS Appl Mater Interfaces 3(9):3725–3731. doi:10.1021/am200913t

Plackett D, Anturi H, Hedenqvist M, Ankerfors M, Gallstedt M, Lindstrom T, Siro I (2010) Physical properties and morphology of films prepared from microfibrillated cellulose and microfibrillated cellulose in combination with amylopectin. J Appl Polym Sci 117(6):3601–3609. doi:10.1002/app.32254

Rennel C, Rigdahl M (1994) Enhancement of the light-scattering ability of coatings by using hollow pigments. Colloid Polym Sci 272(9):1111–1117. doi:10.1007/bf00652380

Ridgway C, Gane P (2012) Constructing NFC-pigment composite surface treatment for enhanced paper stiffness and surface properties. Cellulose 19(2):547–560. doi:10.1007/s10570-011-9634-8

Saarikoski E, Saarinen T, Salmela J, Seppala J (2012) Flocculated flow of microfibrillated cellulose water suspensions: an imaging approach for characterisation of rheological behaviour. Cellulose 19(3):647–659. doi:10.1007/s10570-012-9661-0

Schütz C, Sort J, Bacsik Z, Oliynyk V, Pellicer E, Fall A, Wågberg L, Berglund L, Bergström L, Salazar-Alvarez G (2012) Hard and transparent films formed by nanocellulose–TiO_2 nanoparticle hybrids. PLoS One 7(10):e45828. doi:10.1371/journal.pone.0045828

Segal L, Creely JJ, Martin AE Jr, Conrad CM (1959) An empirical method for estimating the degree of crystallinity of native cellulose using the X-ray diffractometer. Text Res J 29:786–794. doi:10.1177/004051755902901003

Siqueira G, Bras J, Dufresne A (2010) Cellulosic bionanocomposites: a review of preparation. Properties and applications. Polymers 2(4):728–765

Siró I, Plackett D (2010) Microfibrillated cellulose and new nanocomposite materials: a review. Cellulose 17(3):459–494. doi:10.1007/s10570-010-9405-y

Siro I, Plackett D, Hedenqvist M, Ankerfors M, Lindstrom T (2011) Highly transparent films from carboxymethylated microfibrillated cellulose: the effect of multiple homogenization steps on key properties. J Appl Polym Sci 119(5):2652–2660. doi:10.1002/app.32831

Spence KL, Venditti RA, Habibi Y, Rojas OJ, Pawlak JJ (2010) The effect of chemical composition on microfibrillar cellulose films from wood pulps: mechanical processing and physical properties. Bioresour Technol 101(15):5961–5968. doi:10.1016/j.biortech.2010.02.104

Spence KL, Venditti RA, Rojas OJ, Pawlak JJ, Hubbe MA (2011) Water vapor barrier properties of coated and filled microfibrillated cellulose composite films. BioResources 6:4370–4388

Syverud K, Stenius P (2009) Strength and barrier properties of MFC films. Cellulose 16(1):75–85. doi:10.1007/s10570-008-9244-2

Turbak AF, Snyder FW, Sandberg KR (1983) Microfibrillated cellulose, a new cellulose product; properties, uses, and commercial potential. J Appl Polym Sci: Appl Polym Symp 37:815–827

Vilela C, Freire CSR, Marques PAAP, Trindade T, Pascoal Neto C, Fardim P (2010) Synthesis and characterization of new CaCO3/cellulose nanocomposites prepared by controlled hydrolysis of dimethylcarbonate. Carbohydr Polym 79(4):1150–1156. doi:10.1016/j.carbpol.2009.10.056

Wu CN, Saito T, Fujisawa S, Fukuzumi H, Isogai A (2012) Ultrastrong and high gas-barrier nanocellulose/clay-layered composites. Biomacromolecules 13(6):1927–1932. doi:10.1021/bm300465d

Xhanari K, Syverud K, Chinga-Carrasco G, Paso K, Stenius P (2011) Structure of nanofibrillated cellulose layers at the o/w interface. J Colloid Interface Sci 356(1):58–62. doi:10.1016/j.jcis.2010.12.083